

A Study of Source Term Estimators in Coupled Finite-Volume/Monte-Carlo Methods with Applications to Plasma Edge Simulations in Nuclear Fusion: Analog and Collision Estimators

Bert Mortier¹, Martine Baelmans² and Giovanni Samaey^{1,*}

¹ NUMA, Dept. Computer Science, KU Leuven, Celestijnenlaan 200A, B-3001 Leuven, Belgium.

² TME, Dept. Mechanical Engineering, KU Leuven, Celestijnenlaan 300, B-3001 Leuven, Belgium.

Received 9 December 2022; Accepted (in revised version) 14 July 2023

Abstract. In many applications, such as plasma edge simulation of a nuclear fusion reactor, a coupled PDE/kinetic description is required. Such systems can be solved with a coupled finite-volume/Monte-Carlo method. Different procedures have been proposed to estimate the source terms in the finite volume part that appear from the Monte Carlo part of the simulation. In this series of papers, we present a systematic (analytical and numerical) comparison of the variance and computational cost of a coherent set of such estimation procedures. The comparison is based on an invariant imbedding procedure, in which systems of ordinary differential equations (ODEs) are derived that quantify the statistical error and computational cost of each estimator. In this paper, we discuss analog and collision simulation and estimation procedures. We analyze in detail a scenario with forward-backward scattering in a one-dimensional slab, uncovering and quantifying the effects determining the performance of the estimation procedures.

AMS subject classifications: 65C05, 65L12

Key words: Monte Carlo, reaction rate estimation, invariant imbedding, survival biasing, collision estimator.

1 Introduction

One often encounters situations in which an accurate mathematical description of the processes under study requires coupling a partial differential equation (PDE) of reaction-

*Corresponding author. *Email addresses:* bertmortier@hotmail.com (B. Mortier), martine.baelmans@kuleuven.be (M. Baelmans), giovanni.samaey@kuleuven.be (G. Samaey)

advection-diffusion type to a Boltzmann-type kinetic equation that models a distribution of particles in position-velocity phase space. Examples can be found in applications that are as diverse as bacterial chemotaxis [21], rarified gas dynamics [28], and plasma physics [20, 26, 29]. The motivating application in the present work is the simulation of the plasma edge in fusion energy devices, which is of crucial importance to evaluate vital aspects of reactor operation: energy and particle exhaust, as well as erosion of the plasma-facing components and the related migration and deposition of material [12, 20, 26]. In this application, the PDE part of the model describes the plasma, whereas the kinetic equation describes the behaviour of neutral particles.

Such a coupled simulation presents a computational problem due to the different dimensionality of both parts of the model. Both the plasma model and the neutral model can be simulated with either deterministic or stochastic methods, including but not limited to Galerkin methods [10], discrete velocity methods [18], particle-in-cell methods [3], and particle-tracing methods [16]. This work focuses on particle-tracing methods for the neutral kinetic model as they are used in the fusion codes EIRENE [20] and DEGAS2 [27]. These codes can be coupled with, for instance, the deterministic B2 [20] or UEDGE [5] codes or the stochastic EMC3 code [4] for the plasma equations.

In this paper, we start from a prototypical model of this type that appears in plasma edge simulations in nuclear fusion reactors, such as ITER [30]. In this model, the plasma is discretized with a finite volume method, whereas the neutral particles are simulated via Monte Carlo method. Plasma and neutral particles interact through *ionization* and *charge-exchange* events [26], of which the rates depend on the plasma state. During ionization, a neutral particle is ionized and is absorbed by the plasma; ionization is therefore also called absorption in this text. Charge-exchange events model collisions of a neutral particle with an ion during which an electron is transferred from the neutral particle to the ion: the neutral particle then becomes ionized, whereas the ion becomes neutral. In a Monte Carlo simulation, this effect can be emulated by keeping the same neutral particle with a newly sampled velocity; charge-exchange events are therefore also called scattering events. The corresponding Monte Carlo particle tracking simulations are described in Section 2.

During these interactions, mass, momentum, and energy are exchanged between plasma and neutral particles. The exchanges between neutrals and plasma are modeled as source terms in the plasma equations and estimating these source terms is the aim of the neutral model simulation. Given the importance of accurate source term estimation, many estimation procedures have been proposed. Because the source term estimation procedures only trace a finite number of particles, they induce a statistical error and a finite sampling bias on the coupled PDE/Monte-Carlo simulation. Both the statistical error and the finite sampling bias scale with the variance on the source term estimation in the Monte Carlo simulation [6]. Selecting the best estimator, that keeps this variance low for a reasonable computational cost, is thus an important objective [11].

Currently, only a few works are available that compare the performance of source term estimation procedures, usually in a very restrictive setting, leaving the choice of

estimation procedure to the preference or experience of the user. A first important comparison of the estimation procedures was conducted in [17], where an invariant imbedding methodology [1] is used to derive ODEs for the statistical error of a limited set of estimation procedures in a one-dimensional forward scattering scenario. In this degenerate scenario, neutrals always have the same velocity and do not change direction, leading to very simple particle paths. Indira [7] performed a similar study that included forward-backward scattering, but limited the study to estimation procedures for leakage, the number of particles that leave the domain. Both the setting in [17] and [7] allowed for significant simplifications, resulting in ODEs for the statistical error with a comprehensive analytical solution. We also refer to the work of Lux for approximate formulas for the variance of the most commonly used estimators [15], and for sufficient conditions for one estimator to outperform an other one [14]. While useful, Lux' results do not capture the highly non-trivial behaviour at high scattering rates and low absorption rates, where the paths are generally the most complex. For completeness, we also refer to [8, 9, 22–24], in which analytical calculations of the variance are presented to optimize importance sampling.

This paper forms a next step in the systematic study of source term estimators in coupled finite-volume/Monte-Carlo methods. In particular, we discuss the different procedures that can be used for the Monte Carlo estimation of the mass, momentum, and energy source terms, and analyze their variance and computational cost as a function of the plasma background. Due to evolutions in fusion reactor design that push towards so-called detached regimes with high collision rates, the Monte Carlo simulations have often become the computational bottleneck in these simulations. These conditions therefore require careful selection of the most suitable Monte Carlo estimation procedure, or (potentially) the use of different estimation procedures in different parts of the space-time domain.

The main contributions of this paper are the following:

- From a theoretical viewpoint, we gather and propose a classification for the different procedures that are available in the literature to generate particle trajectories and to estimate their contributions to the mass, momentum, and energy sources. In this paper, we treat analog and collision simulations, which are presented with the kinetic model in Section 2, as well as the corresponding estimation procedures, which are presented in Section 3.
- From a numerical analysis viewpoint, we assess the efficiency of these Monte Carlo estimation procedures, with a focus on the estimation of mass. We extend the numerical analysis of these Monte Carlo estimation procedures to anisotropic forward-backward scattering in a one-dimensional slab. To this end, we use an invariant imbedding [1] procedure to construct ODEs for the variance and computational cost of the different estimators, which is described shortly in Section 4. The full derivations, being extremely lengthy, can be found in the Technical Report [19]. The systems of ODEs that result from the invariant imbedding procedure are solved nu-

merically. In Section 5 we use these numerical solutions for different values of the model parameters to discuss the performance of each estimation procedure. As measures of performance, we consider both variance and computational cost.

The remainder of the paper is organised as follows. In Section 2, we discuss the coupled kinetic model that will be used throughout this manuscript, as well as two Monte Carlo simulation strategies for this model. In Section 3, we present two of the basic estimators to extract the quantities of interest from the simulations of Section 2. Then, in Section 4, we present and illustrate the analytical method with which we study the simulation-estimator combinations. In Section 5 we then discuss how the different estimators perform throughout the parameter space.

2 Kinetic neutral model

The neutral particles are modeled in the one-dimensional plasma edge domain $\mathcal{D} = [0, L]$ of length L . In Section 2.1, we first describe the underlying particle model that governs the dynamics of the neutral particle population. From this description, a Monte Carlo simulation method follows trivially, which is called the *analog* simulation method, because the Monte Carlo particles behave analogous to physical particles. We then give an equivalent population-level description, the corresponding Boltzmann-BGK equation, in Section 2.2. We proceed with an alternative particle discretization of the Boltzmann-BGK equation in Section 2.3 that does not explicitly execute ionization reactions, but uses reweighing at scattering events to capture its effects in an unbiased manner. We refer to this particle discretization as the *non-analog collision type* simulation.

While the particle physics has been extensively described in [16], the precise mathematical description of the analog and non-analog particle discretizations, as presented here, does not appear in this detail in the literature. The presentation here is a one-dimensional simplification of the software implementation that is available in [20] and [30].

2.1 Particle-based model

We provide a mathematical description of the behaviour of individual trajectories of neutrals, and consequently also of analog Monte Carlo particles. We consider the plasma state fixed, and thus regard it as a background against which the neutral particles move.

Neutrals arise mostly due to collisions of plasma particles with the divertor target, which is located at $x = 0$ in our domain \mathcal{D} . There are also volumetric sources, due to recombination of the plasma, and external sources. The entire source is denoted as $q(x)$ and the initial velocity distribution is $\hat{f}_0(v|x)$.

We sample the initial position x_0 from

$$\frac{q(x)}{\int q(x)dx'} \quad (2.1)$$

and launch the particle from that position with velocity v_0 , sampled from $\hat{f}_0(v|x_0)$. Both $q(x)$ and $\hat{f}_0(v|x_0)$ are determined by the plasma.

In this paper, we will consider two velocity models. The first model, referred to as *1D1D*, allows continuous velocities and has a continuous initial probability density function with the shape of a shifted Maxwellian. The second model, dubbed *1D0D*, or forward-backward scattering model, only has a single speed v_0 , which results in particles having either v_0 or $-v_0$ as a velocity. This translates into an initial velocity distribution $\hat{f}_0(v|x_0)$ which consists of the sum of two dirac deltas for fixed x_0 . The *1D0D* case is introduced to facilitate the invariant imbedding procedure discussed in Section 4.

Combined, we can regard the initial state of the neutral to be sampled as

$$(x_0, v_0) \sim f_0(x, v) = \frac{q(x)}{\int q(x) dx} \hat{f}_0(v|x) = \frac{Q(x, v)}{\int q(x) dx}. \quad (2.2)$$

After being launched, the particles move through the domain while undergoing a series of events, which can be of two types: collisions and boundary hits. Collisions can be either absorption (ionization) or scattering (charge-exchange), and are a result of interactions with the background plasma. Boundary hits occur whenever a particle hits the boundary $\partial\mathcal{D} = \{0, L\}$: the particle can then either leave the domain or reflect back into the domain. Each particle undergoes a sequence of scattering collisions and boundary reflections until it is either absorbed or leaves the domain via the boundary.

Equations of motion. The state of the particle is represented as a function $t \in [0, T_{\text{end}}] \mapsto (x(t), v(t))$, with the initial time $T_0 = 0$, initial position $x(0) = x_0$, and initial velocity $v(0) = v_0$ given by Eq. (2.2). The particle moves according to a velocity jump process, in which the velocity of the particle only changes at discrete times. Eqs. (2.3)-(2.5) describe this process:

$$x(0) = x_0, \quad (2.3)$$

$$\frac{dx(t)}{dt} = v(t), \quad (2.4)$$

$$v(t) = v_k \text{ for } t \in [T_k, T_{k+1}), \quad k \in \{0, \dots, K-1\}. \quad (2.5)$$

The T_k form the event times and $T_K = T_{\text{end}}$ is the time instance at which the final event occurs and the particle disappears from the simulation. This final event can either be an absorption collision or the particle leaving the domain through the boundary. The velocity at this time instance does not change, $v(T_K) = v_{K-1}$. We now proceed to specify the event times $\{T_k\}_{k=1}^{K-1}$, the behaviour at the different events, including the choice of the velocities v_k , and the end time T_K .

Event times. The event times form an increasing sequence $\{T_k\}_{k=1}^K$ of time instances at which either a collision or a boundary hit occurs. It is only at these time instances

that the velocity changes or the particle disappears. We first consider collision times. Collisions are either scattering or absorption events. The absorption events model reactions between neutral particles and electrons in the plasma (with density $n_e(x)$) that result in ionizing the neutral particles. Scattering events model reactions between the neutral particles and the ions in the plasma (with density $n_i(x)$) that result in an exchange of an electron between neutral particles and ions. We assume the electron and ion densities to be equal, i.e., $n_e(x) \equiv n_i(x)$. The respective rate coefficients of these two reactions are $K_a(x)$ and $K_s(x)$, implying that the probability of a particle undergoing absorption (resp., scattering) during an infinitesimal time dt is $R_a(x)dt = K_a(x)n_e(x)dt$ (resp., $R_s(x)dt = K_s(x)n_i(x)dt$). Note that the rate coefficients K_a, K_s depend on the types of particles involved, whereas the collision rates R_a, R_s also depend on the plasma state.

Writing the total collision rate as $R_t(x) = R_a(x) + R_s(x)$, the next collision time T_{k+1}^c can be obtained from an exponential distribution with time-dependent rate and computed by solving

$$\int_{T_k}^{T_{k+1}^c} R_t(x(t)) dt = \epsilon_{k+1}, \quad (2.6)$$

for T_{k+1}^c , with ϵ_k a standard exponentially distributed random number, i.e.,

$$\epsilon_k \sim \mathcal{E}(1). \quad (2.7)$$

The resulting probability distribution of the time $\Delta t_k^c = T_{k+1}^c - T_k$ to the next collision is then given by

$$P(\Delta t_k^c | x(T_k), v_k) = R_t(x(T_k + \Delta t_k^c)) \exp\left(-\int_0^{\Delta t_k^c} R_t(x(T_k + \tau)) d\tau\right). \quad (2.8)$$

In the absence of collision events, the particle would hit the boundary of the domain at time T_{k+1}^b , which depends deterministically upon $x(T_k)$ and $v(T_k)$:

$$T_{k+1}^b = T_k + \min(\tau | \tau > 0, x(T_k) + \tau v(T_k) \in \partial\mathcal{D}). \quad (2.9)$$

Given the above processes, the next event, that marks the end of the current flight path, occurs at time

$$T_{k+1} = \min(T_{k+1}^c, T_{k+1}^b). \quad (2.10)$$

We define convenient auxiliary variables b_{k+1} and c_{k+1} that encode whether the event was a boundary hit or a collision.

$$(c_{k+1}, b_{k+1}) = \begin{cases} (1, 0) & \text{if } T_{k+1}^c \leq T_{k+1}^b \quad (\text{collision}), \\ (0, 1) & \text{if } T_{k+1}^c > T_{k+1}^b \quad (\text{boundary hit}). \end{cases} \quad (2.11)$$

Remark 2.1 (Practical sampling of the next collision time, T_{k+1}^c). In a practical simulation, the plasma state (and thus also $R_t(x)$) is only available on a grid [20], and will be treated as piecewise constant. Then, Eq. (2.6) allows sampling of T_{k+1}^c quite easily. With the index

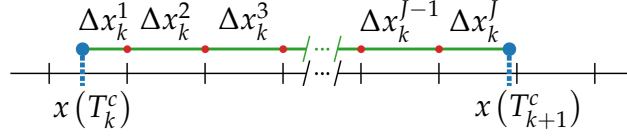


Figure 1: A sketch showing the path of a particle from event k on the left, to the next collision at time T_{k+1}^c . Intermediate grid cell crossings are indicated with red dots.

j referring to the grid cells in the order the particle moves through them, a piecewise constant reaction rate allows to rewrite Eq. (2.6) as

$$\sum_{j=0}^J R_t^j \Delta t_k^j = \epsilon_{k+1}. \quad (2.12)$$

The Δt_k^j refer to the time spent in the j -th encountered grid cell. Because the particle has constant velocity between events, the time Δt_k^j spent in passing grid cell j equals the distance Δx_k^j to the edge of the grid cell divided by the size of the velocity $|v_k|$, hence Eq. (2.12) can be rewritten as

$$\sum_{j=0}^J R_t^j \frac{1}{|v_k|} \Delta x_k^j = \epsilon_{k+1}. \quad (2.13)$$

The meaning of Δx_k^j is illustrated in Fig. 1.

In practice, sampling of the time or distance to the next collision is done by calculating the distances to the subsequent grid cell walls until their weighted sum, as in Eq. (2.13), exceeds ϵ_{k+1} . The last value, Δt_k^J or Δx_k^J , can be found by solving Eq. (2.12), respectively Eq. (2.13), exactly.

Remark 2.2 (Distance to the next collision.). The bijection between Δt_k and Δx_k as discussed in Remark 2.1 can be used to disregard event times in the description of a particle path, only retaining the event positions and velocities [16]. Similarly to the probability distribution of the next collision time in Eq. (2.8), we can express the probability distribution of the travelled distance d to the next collision as:

$$P(d|x, v) = \frac{R_t(x + d \frac{v}{|v|})}{|v|} e^{-\int_0^d \frac{R_t(x + \ell \frac{v}{|v|})}{|v|} d\ell}. \quad (2.14)$$

In our description of the particle paths of this section, we will hold on to the event times, as this forms the most natural description of the particle path. In later sections, the description in Eq. (2.14) will be more convenient.

Remark 2.3 (Cross-sections.). An often-used different parameter to express the collisionality is the cross-section Σ . It is defined as

$$\Sigma(x, v) = \frac{R(x)}{|v|}, \quad (2.15)$$

and expresses the expected number of events per distance travelled.

With $\Sigma_t(x, v) = \Sigma_a(x, v) + \Sigma_s(x, v)$ the total cross-section, the probability distribution (2.14) of the travelled distance d to the next collision can also be written as

$$P(d|x, v) = \Sigma_t(x + dv/|v|, v) e^{-\int_0^d \Sigma_t(x + \ell v/|v|, v) d\ell}. \quad (2.16)$$

Collision events. If a collision occurs at time T_{k+1} ($c_{k+1} = 1$), the collision is either an absorption, with probability $R_a(x(T_{k+1}))/R_t(x(T_{k+1}))$, or a scattering otherwise. The type of collision is decided by generating a Bernoulli distributed random number:

$$a_{k+1} \sim \mathcal{B}\left(\frac{R_a(x_{k+1})}{R_t(x_{k+1})}\right). \quad (2.17)$$

If $a_{k+1} = 1$, absorption occurs, which means the particle path ends. The index of the last collision event, would then thus be

$$K_a = \min(k | c_k a_k = 1). \quad (2.18)$$

If $a_{k+1} = 0$, a scattering collision takes place, and a new velocity is sampled according to

$$v_{k+1}^s \sim \hat{f}_{\text{postcol}}(v|x(T_{k+1})). \quad (2.19)$$

Remark 2.4 (Fusion-specific postcollision velocity distribution). In the plasma edge simulations we study, the postcollision velocity is independent of the precollision velocity, and completely determined by the plasma background. The theory about the estimation procedures of this paper remains valid in the more general case where the postcollisional velocity distribution does depend on the precollision velocity. This would require changing $\hat{f}_{\text{postcol}}(v|x)$ to $\hat{f}_{\text{postcol}}(v|x, v')$.

The two velocity models, 1D1D and 1D0D, result in two different models for the post-collision velocity distribution, similarly to the two initial velocity distribution shapes presented on page 108. In the 1D1D model, the post-collision velocity is sampled from a normal distribution, whose moments are determined by the plasma properties. In the simplified 1D0D model, where only a single velocity size is allowed, the post-collision velocity only determines the probability of being $-v_0$ or v_0 .

Boundary hits. If the event is a boundary hit ($b_{k+1} = 1$), the particle can either be absorbed at the boundary (with probability $\alpha(x)$), or be reflected (with probability $1 - \alpha(x)$). To select the type of boundary hit, we again generate a Bernoulli distributed variable β_{k+1} :

$$\beta_{k+1} \sim \mathcal{B}(\alpha(x_{k+1})). \quad (2.20)$$

If $b_{k+1} = 1$ and $\beta_{k+1} = 1$, the particle leaves the domain, as is expressed by

$$K_{\text{out}} = \min(k | b_k \beta_k = 1). \quad (2.21)$$

Otherwise, if $b_{k+1} = 1$ and $\beta_{k+1} = 0$, the particle is reflected, which leads to a new deterministic velocity based on its current velocity and the normal to the boundary at the reflection location, via the equation

$$v_{k+1}^r = B(v_k), \quad (2.22)$$

with $B(v) \equiv -v$, a deterministic function that represents perfect reflection at the wall.

New velocity. To summarize, v_{k+1} equals v_{k+1}^s if the next event is a collision ($b_{k+1} = 0$) and v_{k+1}^r if the event is a boundary hit ($b_{k+1} = 1$). Otherwise, the particle velocity does not change. This is expressed by the equation

$$v_{k+1} = c_{k+1}v_{k+1}^s + b_{k+1}v_{k+1}^r. \quad (2.23)$$

Note that if an absorption takes place ($c_{k+1}a_{k+1} = 1$) or if the particle leaves the domain ($b_{k+1}\beta_{k+1}$), the velocity v_{k+1} does not play a role.

End time. The particle path ends at the first absorption event or when it leaves the domain, hence

$$K = \min(K_a, K_{\text{out}}), \quad (2.24)$$

$$T_{\text{end}} = T_K = \min(T_{K_a}, T_{K_{\text{out}}}). \quad (2.25)$$

Grid cell crossings. This section provided a full description of particle paths that adhere to the physical model. Such a path is fully characterized by the initial state, the positions of the events, the inter-event velocities, and the types of the events: (x_0, v_0) and $\{x_k, v_k, c_k, b_k, a_k, \beta_k\}_{k=1}^K$. (The event times, which played a central role in this discussion, can be derived from the event positions and velocities, as is discussed in Remark 2.2.) In a practical context, the plasma background is often discretized in a piecewise constant manner, see Remark 2.1, and for some source term estimators it will be relevant to also regard grid cell crossings as events, see Section 3. We may include grid cell crossings by extending the set of events, which until now only comprised collisions and boundary hits. Their treatment can be incorporated in the treatment of boundary hits by augmenting the set $\partial\mathcal{D}$ with $\cup_i \partial\mathcal{C}^i$ in Eq. (2.9) and by including an additional auxiliary variable g_k . At a grid cell crossing $g_k = 1$ and $c_k = b_k = 0$, and at other events $g_k = 0$. For convenience, we also treat the entry of the particle in the domain as a grid cell crossing at $t = 0$.

Analog particle path. The entire particle path can be summarized as

$$\mathcal{P} = \{x_k, v_k, c_k, b_k, g_k, a_k, \beta_k\}_{k=0}^K. \quad (2.26)$$

Simulations that follow the mathematical description of this section are called *analog simulations* and will be denoted by \mathbf{a} in this paper. After introducing a kinetic description of this model in Section 2.2, we will derive a different *non-analog simulation* of the same model in Section 2.1, that loosens the connection to the physical model.

2.2 Kinetic Boltzmann-BGK model

For the analog stochastic process discussed above, one can write a corresponding kinetic equation for the equilibrium distribution $\phi_n(x, v)$ of an infinite number of such particles [16],

$$\underbrace{v \nabla \phi_n(x, v)}_{\text{transport}} = \underbrace{Q(x, v)}_{\text{source from the plasma}} - \underbrace{R_a(x) \phi_n(x, v)}_{\text{sink due to absorption}} + \underbrace{\int R_s(x) \phi_n(x, v') \hat{f}_{\text{postcol}}(v|x) dv'}_{\text{velocity redistribution due to scattering}}. \quad (2.27)$$

The probability of a particle being absorbed during a time dt is equal to $R_a(x)dt$, resulting in a sink of $R_a(x)\phi_n(x, v)$, since absorbed neutrals disappear from the neutral population. Analogously for the scattering events, a fraction $R_s(x)\phi_n(x, v)$ gets scattered. Unlike the absorbed neutrals, they remain in the neutral population: a particle undergoing scattering at position x with precollision velocity v' , remains in the neutral population, but changes velocity according to the velocity distribution $\hat{f}_{\text{postcol}}(v|x)$. This aspect is modeled by the last term of the right hand side of Eq. (2.27).

As in [16], we will split Eq. (2.27) into an event and a transport part to facilitate the derivation of the different source term estimation procedures in Section 3. In [16], the considered events are entry into the domain, absorption collisions, and scattering collisions. In this paper, we add exits at the boundary, reflections at the boundary, and grid cell crossings as events. Our construction derives from the particle-based model of Section 2.1, which is equivalent to Eq. (2.27).

Event part. We introduce the collision rate $\psi_c(x, v)$, the rate at which particles undergo collisions, as

$$\psi_c(x, v) = (R_a(x) + R_s(x)) \phi_n(x, v) = R_t(x) \phi_n(x, v), \quad (2.28)$$

with $R_t(x)$ the total rate. Similarly, we denote by $\psi_b(x, v)$ and $\psi_g(x, v)$ the boundary hit rate and the grid cell crossing rate, which are of course only non-zero at domain, respectively grid cell boundaries. With these event rates, we can write the following equation for the post-event rate $\chi(x, v)$, being the rate at which particles appear after events or due to sources:

$$\chi(x, v) = \underbrace{Q(x, v)}_{\text{entry}} + \underbrace{\int \psi_c(x, v') C(v' \rightarrow v|x) dv'}_{\text{collisions}} + \underbrace{\psi_b(x, B^{-1}(v)) (1 - \alpha(x))}_{\text{boundary interactions}} + \underbrace{\psi_g(x, v)}_{\text{grid cell crossings}}. \quad (2.29)$$

The second term of the right hand side of Eq. (2.29) contains the collision kernel

$$C(v' \rightarrow v|x) = \frac{R_s(x)}{R_t(x)} \hat{f}_{\text{postcol}}(v|x), \quad (2.30)$$

which describes the effect of a collision. Its form in Eq. (2.30) corresponds to the description of collision events in Section 2.1, where a particle that undergoes a collision has a

probability $1 - R_s(x)/R_t(x)$ to be ionized and thus disappear from the neutral simulation, and a probability $R_s(x)/R_t(x)$ of reappearing with a new velocity that is sampled according to the distribution $\hat{f}_{\text{postcol}}(v|x)$, see Eqs. (2.19) and (2.17). The third term of the right hand side of Eq. (2.29) represents that particles that hit a boundary with a velocity $B^{-1}(v)$ will end up with a velocity v after the boundary hit with the reflection probability $(1 - \alpha(x))$. (They disappear from the domain with a probability $\alpha(x)$, also in correspondence with the boundary hits description of Section 2.1, see Eqs. (2.20) and (2.22).) At a grid cell crossing, the velocity of the particle does not change, as this is not a physical event. Therefore, the disappearing particles $\psi_g(x, v)$ simply reappear unaltered.

Transport part. Eqs. (2.29)-(2.30) describe the result of events. We still need to describe the effect of particle transport, which will connect the post-event rate $\chi(x, v)$ to the event rates, $\psi_c(x, v)$, $\psi_b(x, v)$, and $\psi_g(x, v)$. Together with Eqs. (2.29)-(2.30), the transport description presented below will give rise to a closed set of equations. Particles arising at position x' with velocity v move to their next event position x . This transport phase is modelled by transport kernels $T_e(x' \rightarrow x|v)$, which express the probability of a particle that entered the simulation or resulted from a previous event at position x' with velocity v' , to undergo a next event at x . We split the transport kernel into two parts: $T_c(x' \rightarrow x|v)$ that expresses the probability of undergoing a collision, and $T_{\text{geom}}(x' \rightarrow x|v)$ that expresses the probability of a geometric event, which groups boundary hits and grid cell crossings. The total transport kernel is $T(x' \rightarrow x|v) = T_c(x' \rightarrow x|v) + T_{\text{geom}}(x' \rightarrow x|v)$. With these two kernels, equations for the event rates are:

$$\psi_c(x, v) = \int \chi(x', v) T_c(x' \rightarrow x|v) dx', \quad (2.31)$$

$$\psi_b(x, v) = \int \chi(x', v) T_{\text{geom}}(x' \rightarrow x|v) \mathbf{1}_{\partial\mathcal{D}}(x) dx', \quad (2.32)$$

$$\psi_g(x, v) = \int \chi(x', v) T_{\text{geom}}(x' \rightarrow x|v) (1 - \mathbf{1}_{\partial\mathcal{D}}(x)) dx'. \quad (2.33)$$

$\mathbf{1}_{\partial\mathcal{D}}$ is an indication function that is one domain boundaries and zero otherwise. Eq. (2.31) connects back to Eq. (2.14) which gives the probability distribution of the distance to the next collision event. Using Eq. (2.14), the following equation for the collision transport kernel is obtained for the case without any geometric event:

$$T_{c,\infty}(x' \rightarrow x|v) dx = \begin{cases} \frac{R_t(x)}{|v|} e^{-\int_0^d \frac{R_t(x' + \ell \frac{v}{|v|})}{|v|} d\ell} dd & \text{if } x = x' + D \frac{v}{|v|} \text{ with } D \geq 0, \\ 0 & \text{else.} \end{cases} \quad (2.34)$$

In Section 2.1, a collision only occurred when the particle did not hit the boundary first. We add this to Eq. (2.34) to get the actual collision transition kernel

$$T_c(x' \rightarrow x|v) dx = \begin{cases} \frac{R_t(x)}{|v|} e^{-\int_0^d \frac{R_t(x' + \ell \frac{v}{|v|})}{|v|} d\ell} dd & \text{if } x = x' + D \frac{v}{|v|} \text{ with } D \geq 0 \text{ and} \\ & x \text{ and } x' \text{ are in the same grid cell,} \\ 0 & \text{else.} \end{cases} \quad (2.35)$$

For completeness we include a single-line expression for $T_c(x' \rightarrow x|v)$. In a one-dimensional setting, the distance (D) equals the difference in the position (x) times the sign of the velocity ($\frac{v}{|v|}$). Hence, we have $\frac{v}{|v|} dx = dD$, and we can implement the first part of the if-else switch in Eq. (2.35) by multiplication with a factor $\frac{1}{2} \left| \frac{x-x'}{|x-x'|} + \frac{v}{|v|} \right|$. The second part of the if-else switch is added by multiplication of $\max_j (\mathbf{1}_{C^j}(x) \mathbf{1}_{C^j}(x'))$, which is one only if x and x' are in the same grid cell and zero otherwise. The resulting single-line expression for the collision transport kernel is

$$T_c(x' \rightarrow x|v) = \frac{1}{|v|} R_t(x) e^{-\int_{x'}^x \frac{v}{|v|^2} R_t(x'') dx''} \frac{1}{2} \left| \frac{x-x'}{|x-x'|} + \frac{v}{|v|} \right| \max_i (\mathbf{1}_{C^i}(x) \mathbf{1}_{C^i}(x')). \quad (2.36)$$

If the next event of a particle is not a collision, it is either a grid cell crossing or a boundary hit. The probability of having either of these geometric events as the next event equals the probability of not colliding before reaching a grid cell boundary or domain boundary, hence the total probability of a geometric event equals

$$\int T_{\text{geom}}(x' \rightarrow x|v) dx = 1 - \int T_c(x' \rightarrow x|v) dx, \quad (2.37)$$

where $T_{\text{geom}}(x' \rightarrow x|v)$ is the geometric transition kernel, combining grid cell crossings and boundary hits. The position x of the next geometric event is always the first position on a boundary (a domain boundary, or grid cell boundary) that is reached when continuing along the line $x' + v\tau, \tau > 0$. With

$$\Theta(x', v) = \min(\tau | \tau > 0, x' + v\tau \in \cup_i \partial C^i), \text{ with } \partial \mathcal{D} \subset \cup_i \partial C^i, \quad (2.38)$$

the time after which the boundary would be reached, and similar to Eq. (2.9), we can express the position at which a geometric event takes place as $x' + v\Theta(x', v)$. Consequently, the geometric transition kernel is

$$\begin{aligned} T_{\text{geom}}(x' \rightarrow x|v) &= \left(1 - \int_{x'}^x T_c(x' \rightarrow x''|v) dx'' \right) \delta(x - x' - v\Theta(x', v)) \\ &= \left(1 - \int_{x'}^x \frac{v}{|v|^2} R_t(x'') e^{-\int_{x'}^{x''} \frac{v}{|v|^2} R_t(x''') dx'''} dx'' \right) \delta(x - x' - v\Theta(x', v)) \\ &= e^{-\int_{x'}^x \frac{v}{|v|^2} R_t(x'') dx''} \delta(x - x' - v\Theta(x', v)). \end{aligned} \quad (2.39)$$

Eqs. (2.29), (2.31), (2.32), and (2.33), combined with the expressions for the kernels in Eqs. (2.30), (2.36), and (2.39), form a closed set of integral equations for $\psi_c(x, v)$.

2.3 Non-analog collision type simulation

In the analog simulation of neutral particles, it often occurs that certain regions of the domain have a very low probability of being reached, for instance due to high absorption rates in surrounding regions. In non-analog simulations, this situation is circumvented by considering weighted particles, introducing a so-called survival biasing procedure [13]. In such methods, absorption is not executed by letting the particle disappear,

but by adapting its weight instead. This way, particles are much more likely to traverse regions with a high absorption probability, a ‘survival bias’ that is compensated by a decrease of the particle weight to maintain unbiasedness of the simulation.

In the analog situation, there is a probability of $R_a(x)/R_t(x)$ to be absorbed at collisions (which means the particle is gone from the simulation) and a probability of $R_s(x)/R_t(x)$ to be scattered. One can therefore also decide to execute a scattering event at each collision, regardless of the type, while simultaneously adjusting the weight with a factor $R_s(x)/R_t(x)$. The resulting simulation is called a collision simulation.

Kinetic description. When regarding Eqs. (2.29) and (2.30), the particle paths generated by the model of this section can be interpreted as changing only how the collision kernel $C(v' \rightarrow v|x)$ is applied with respect to the model in Section 2.1. Instead of having probability $R_a(x)/R_t(x)$ of taking the particle out of the simulation and probability $R_s(x)/R_t(x)$ of the particle undergoing a scattering event, one always performs a scattering event, but multiplies the particle’s weight by $R_s(x)/R_t(x)$. This process thus leads to exactly the same equation for the densities $\psi_c(x,v)dxdv$, $\psi_b(x,v)dxdv$, $\psi_g(x,v)dxdv$, and $\chi(x,v)dxdv$ as the process described in Section 2.1, so sampling at events in this simulation type samples the same measure.

Particle description. With minor changes, the model in Section 2.1 can be adapted to represent this altered simulation process. We will elaborate the entire non-analog collision type model in Eqs. (2.40)-(2.57) and indicate changes with respect to the analog model of Section (2.1) with a shaded background. Now, a particle path is represented as a function $t \in [0, T_{\text{end}}] \mapsto (\bar{x}(t), \bar{v}(t), \bar{w}(t))$, which includes a weight function. The initial state of the particle now also contains a deterministic initial weight, set to 1. The initial state is now determined as

$$(\bar{x}_0, \bar{v}_0) \sim f_0(x, v) = \frac{Q(x)}{\int Q(x) dx} \hat{f}_0(v|x), \quad (2.40)$$

$$\bar{w}_0 = 1. \quad (2.41)$$

Just as the velocity function, the weight function is only updated at events, resulting in a similar equation for $\bar{w}(t)$ as for $\bar{v}(t)$:

$$\bar{x}(0) = \bar{x}_0, \quad (2.42)$$

$$\frac{d\bar{x}(t)}{dt} = \bar{v}(t), \quad (2.43)$$

$$\bar{v}(t) = \bar{v}_k \text{ for } t \in [\bar{T}_k, \bar{T}_{k+1}[, \quad k \in \{0, \dots, \bar{K}-1\}, \quad (2.44)$$

$$\bar{w}(t) = \bar{w}_k \text{ for } t \in [\bar{T}_k, \bar{T}_{k+1}[, \quad k \in \{0, \dots, \bar{K}-1\}. \quad (2.45)$$

As before, $\bar{v}(\bar{T}_{\bar{K}}) = \bar{v}_{\bar{K}-1}$ and $\bar{w}(\bar{T}_{\bar{K}}) = \bar{w}_{\bar{K}-1}$.

The weight updates replace the execution of absorption collisions with scattering collisions. Hence the equations that express absorption in an analog simulation (Eqs. (2.17) and (2.18)) are no longer included in the collision type non-analog (nac) model. The resulting survival bias is mitigated by the weight updates at collisions as expressed by Eq. (2.52) to obtain an unbiased simulation. We thus get the following set of equations for the sampling of events:

$$\bar{\theta}_{k+1} \sim \mathcal{E}(1), \quad (2.46)$$

$$\int_{\bar{T}_k}^{\bar{T}_{k+1}^c} R_t(\bar{x}(t)) dt = \bar{\theta}_{k+1}, \quad (2.47)$$

$$\bar{T}_{k+1}^b = \bar{T}_k + \min(\tau | \tau \geq 0, \bar{x}(\bar{T}_k) + \tau \bar{v}(\bar{T}_k) \in \partial\mathcal{D}), \quad (2.48)$$

$$\bar{T}_{k+1} = \min(\bar{T}_{k+1}^c, \bar{T}_{k+1}^b), \quad (2.49)$$

$$(\bar{b}_{k+1}, \bar{c}_{k+1}) = \begin{cases} (1, 0) & \text{if } \bar{T}_{k+1}^c \leq \bar{T}_{k+1}^b \quad (\text{collision}), \\ (0, 1) & \text{if } \bar{T}_{k+1}^c > \bar{T}_{k+1}^b \quad (\text{boundary hit}), \end{cases} \quad (2.50)$$

$$\bar{v}_{k+1}^s \sim \hat{f}_{\text{postcol}}(v | \bar{x}(\bar{T}_{k+1})), \quad (2.51)$$

$$\bar{w}_{k+1} = \bar{w}_k \left(1 - \bar{c}_{k+1} \frac{R_a(\bar{x}(\bar{T}_{k+1}))}{R_t(\bar{x}(\bar{T}_{k+1}))} \right), \quad (2.52)$$

As a consequence of the absence of absorption, the last event will always be a boundary hit in which the particle leaves the domain, expressed by Eqs. (2.55) and (2.57), which replace Eqs. (2.21) and (2.25) from Section 2.1. The equations modeling boundary hits and the new velocity and end time, therefore become:

$$\bar{\beta}_{k+1} \sim \mathcal{B}(\alpha(\bar{x}_{k+1})), \quad (2.53)$$

$$\bar{v}_{k+1}^r = B(\bar{v}_k), \quad (2.54)$$

$$\bar{K} = \bar{K}_{\text{out}} = \min(k | \bar{b}_k \bar{\beta}_k = 1), \quad (2.55)$$

$$\bar{v}_{k+1} = \bar{c}_{k+1} \bar{v}_{k+1}^s + \bar{b}_{k+1} \bar{v}_{k+1}^r, \quad (2.56)$$

$$\bar{T}_{\text{end}} = \bar{T}_K, \quad (2.57)$$

with \hat{f}_{postcol} the post-collision velocity distribution and $B(v) \equiv -v$.

Due to its focus on the collision events, this type of simulation will be called the *non-analog collision type simulation* in subsequent sections and will be denoted by *nac*.

Remark 2.5 (Reweighting at the boundary). A logical extension is to apply reweighting also at boundary hits, by reweighting the particle with its probability of surviving. Doing so would mean the particle has no more means of disappearing from the simulation, which is solved in practice by using either a cut-off weight below which the particle disappears, Russian roulette, or a similar strategy [16].

As for the analog simulation, it suffices to only keep the path information at the events to perform a Monte Carlo estimation. As before, we include grid cell crossings and the

initial entry into the domain, which have $\bar{g}_k = 1$ and $\bar{c}_k = \bar{b}_k = 0$. The non-analog collision type path can be represented as

$$\bar{\mathcal{P}} = \{\bar{x}_k, \bar{v}_k, \bar{c}_k, \bar{b}_k, \bar{g}_k, \bar{w}_k, \bar{\beta}_k\}_{k=0}^K. \quad (2.58)$$

Note that the absorption indicators a_k are replaced by weights \bar{w}_k compared to Section 2.1.

Remark 2.6 (Simulations with a piecewise constant plasma background). In practical fusion simulations, the neutral particles of the Monte Carlo simulation usually move against a piecewise constant plasma background, as is discussed in Remark 2.1. This facilitates sampling of the next event times by transforming the integral in Eq. (2.6) or (2.47) to a sum. For both the analog simulation (a) as the non-analog collision type simulation (nac), this is the only simplification with respect to the general plasma model.

3 Source term estimation procedures

The purpose of the particle simulations in Sections 2.1 and 2.3 is to estimate transfer of mass, momentum, and energy from the neutral particles to the plasma. To achieve this, one additionally needs source term estimation procedures, which we introduce in this section. The analysis of the variance and computational cost of these estimation procedures forms the core of the paper. Since the source terms in the plasma equations arise from collisions between the neutrals and the plasma, we can express them in terms of the collision rate distribution $\psi_c(x, v)$, see Eq. (2.29), as

$$S_*(x) = \int \left(\frac{R_a(x)}{R_t(x)} s_{a,*}(v) + \frac{R_s(x)}{R_t(x)} \int s_{s,*}(v \rightarrow v') \hat{f}_{\text{postcol}}(v'|x) dv' \right) \psi_c(x, v) dv, \quad (3.1)$$

with $s_{a,*}(v)$ the source contribution due to an absorption of a particle with velocity v and $s_{s,*}(v \rightarrow v')$ the source contribution due to a particle with velocity v scattering with a resulting velocity v' .

The precise functions $s_{a,*}(v)$ and $s_{s,*}(v \rightarrow v')$ depend on the quantity that is being estimated. The mass source from the neutrals to the plasma for instance only arises due to absorption events, and at absorption events the full mass of the particle is transferred to the plasma. This is expressed by $s_{a,\text{mass}}(v) = 1$ and $s_{s,\text{mass}}(v \rightarrow v') = 0$, resulting in

$$S_{\text{mass}}(x) = \int \frac{R_a(x)}{R_t(x)} \psi_c(x, v) dv, \quad (3.2)$$

as the mass source. The momentum source arises from both absorption and scattering collisions. At absorption collisions the entire momentum, proportional to v , is transferred. At scattering collisions, the transferred momentum is proportional to the pre-collisional velocity v minus the post-collisional velocity v' . For each possible outcome v' of a scattering collision of a particle with velocity v , the transferred momentum, which

is proportional to $(v - v')$, has to be multiplied by the probability of having v' as a post-collisional velocity. This results in $s_{a,\text{mom}}(v) = v$, $s_{s,\text{mom}}(v \rightarrow v') = v - v'$, and

$$S_{\text{mom}}(x) = \int \left(\frac{R_a(x)}{R_t(x)} v + \frac{R_s(x)}{R_t(x)} \int (v - v') \hat{f}_{\text{postcol}}(v'|x) dv' \right) \psi_c(x, v) dv. \quad (3.3)$$

In a coupled finite-volume/Monte-Carlo simulation, we introduce a finite volume grid with grid cell boundaries $\{x_0 = 0, x_1, x_2, \dots, x_{I-1}, x_I = L\}$. We are interested in the value of the source terms in each of the I grid cells $C^i = [x_{i-1}, x_i]$, $i = 1 \dots I$. We obtain these source terms by multiplying the functions $s_a(v)$ and $s_s(v \rightarrow v')$ with the characteristic function $\mathbf{1}_{C^i}(x)$ of the grid cell,

$$S_*^i = \int \left(\frac{R_a(x)}{R_t(x)} s_{a,*}(v) + \frac{R_s(x)}{R_t(x)} \int s_{s,*}(v \rightarrow v') \hat{f}_{\text{postcol}}(v'|x) dv' \right) \mathbf{1}_{C^i}(x) \psi_c(x, v) dv dx. \quad (3.4)$$

A Monte Carlo approximation replaces Eq. (3.4) by contributions at events, averaged over N particle paths $\{\mathcal{P}_n\}_{n=1}^N$, see Eqs. (2.26) and (2.58) for the definition of the particle paths. The subscript $n = 1, \dots, N$ denotes the particle index. Note that the number of events that each particle undergoes can depend on the particle's index, so we denote this number of events as $K - n$. In general, each of the $K + 1$ events of a particle path can result in a *score* for the source term estimator in the grid cell i . Depending on the event type, the scoring can differ. In general, we denote the score at an event as $s_{e,*}^{i,*}$, with the superscript $*$ serving as a place-holder for the estimator type, the e for the event type, and the subscript $*$ for the estimated quantity. Precise definitions of these scores are given in Section 3.1 for analog estimators and in Section 3.2 for collision estimators. The resulting Monte Carlo estimator then reads

$$S_*^{i,*} = \frac{1}{N} \sum_{n=1}^N \sum_{k=0}^{K^n} \left(\underbrace{s_{a,*}^{i,*}(\mathcal{P}^n, k) c_k^n a_k^n}_{\text{absorption}} + \underbrace{s_{s,*}^{i,*}(\mathcal{P}^n, k) c_k (1 - a_k^n)}_{\text{scattering}} \right. \\ \left. + \underbrace{s_{\text{out},*}^{i,*}(\mathcal{P}^n, k) b_k^n (1 - \beta_k^n)}_{\text{boundary absorption}} + \underbrace{s_{r,*}^{i,*}(\mathcal{P}^n, k) b_k^n \beta_k^n}_{\text{boundary reflection}} + \underbrace{s_{g,*}^{i,*}(\mathcal{P}^n, k) c_k^n}_{\text{grid cell crossing}} \right), \quad (3.5)$$

where all the symbols are introduced in Section 2.1. The Monte Carlo approximation in Eq. (3.5) is for analog particle paths. For non-analog particle paths, the scores should be multiplied by the appropriate weight, as will be discussed for each estimator separately.

In Section 3.1 we present the *analog estimator* which scores the contributions as they occur within the particle path simulation. In Section 3.2 the *collision estimator* is presented, which will score on more events than only those that occur, in an unbiased fashion. For each estimator, we include an involved example and a discussion of how the estimators reduce in the fundamental cases of estimating the expected number of absorption events and scattering events when the plasma is piecewise-constant. For these fundamental cases, we analytically study the estimation variance and cost in Sections 4 and 5.

3.1 Analog estimator

As discussed in the introduction of this section, an analog MC estimator for S_*^i is the most straightforward estimator from the perspective of an analog simulation. An analog estimator scores according to the physical event that is being simulated. So in an analog simulation, an analog estimator scores

$$s_{a,*}^{i,a}(\mathcal{P}^n, k) = s_{a,*}(v_k) \mathbf{1}_{C^i}(x_k^n) \quad (3.6)$$

at each absorption collision and

$$s_{s,*}^{i,a}(\mathcal{P}^n, k) = s_{s,*}(v_k \rightarrow v_{k+1}) \mathbf{1}_{C^i}(x_k^n) \quad (3.7)$$

at each scattering collision. The superscript a denotes the analog estimator. At other events, there is no physical exchange with the plasma, hence $s_{out,*}^{i,a}(\mathcal{P}^n, k) = s_{r,*}^{i,a}(\mathcal{P}^n, k) = s_{g,*}^{i,a}(\mathcal{P}^n, k) = 0$. Non-analog simulations are not relevant for an analog estimator, since the events lose their physical meaning. We illustrate this estimator type with a momentum estimator:

Example 3.1 (Momentum estimation by an analog estimator in an analog simulation (a.a estimation procedure)). We will show the formula for an estimate of the momentum source in cell i from an analog particle path. The particle path of the n -th particle is represented by the set of positions, incoming velocities and event identification, as given on page 112, at the $K^n + 1$ events of the particle path $\mathcal{P}^n = \{x_k^n, v_k^n, a_k^n, b_k^n, c_k^n\}_{k=0}^{K^n}$. For an analog estimator, only the events at which there is a physically founded interaction with the plasma result in a score, hence if $c_k^n = 1$. For momentum the source at an absorption event is $s_{a,mom}(v) = v$ and at a scattering event it is $s_{s,mom}(v \rightarrow v') = v - v'$. Consequently the terms in Eq. (3.5) become $s_{a,mom}^{i,a}(\mathcal{P}^n, k) = v_k^n \mathbf{1}_{C^i}(x_k^n)$, $s_{s,mom}^{i,a}(\mathcal{P}^n, k) = (v_k^n - v_{k+1}^n) \mathbf{1}_{C^i}(x_k^n)$, and $s_{out,mom}^{i,a}(\mathcal{P}^n, k) = s_{r,mom}^{i,a}(\mathcal{P}^n, k) = s_{g,mom}^{i,a}(\mathcal{P}^n, k) = 0$. All of collisions with the plasma are scattering collisions, except for the last, K^n -th, event, which, if it is a collision, is an absorption. Hence, Eq. (3.5) specifies to

$$S_{mom}^{i,a} = \frac{1}{N} \sum_{n=1}^N \left(\underbrace{\sum_{k=1}^{K^n-1} (v_k^n - v_{k+1}^n) c_k^n \mathbf{1}_{C^i}(x_k^n)}_{\text{scattering collisions}} + \underbrace{v_{K^n}^n c_{K^n}^n \mathbf{1}_{C^i}(x_{K^n}^n)}_{\text{absorption collision}} \right). \quad (3.8)$$

Fundamental cases. We end the description of the analog estimator by applying it to the fundamental cases of estimating the expected number of absorption events and the expected number of scattering events when the plasma is piecewise-constant. These cases correspond to $s_{a,a}(v) = 1$ and $s_{s,a}(v \rightarrow v') = 0$, respectively $s_{a,sc}(v) = 0$ and $s_{s,sc}(v \rightarrow v') = 1$, or thus $s_{a,a}^{i,a}(\mathcal{P}, k) = \mathbf{1}_{C^i}(x_k)$ and $s_{a,sc}^{i,a}(\mathcal{P}, k) = 0$, respectively $s_{a,a}^{i,a}(\mathcal{P}, k) = 0$ and $s_{a,sc}^{i,a}(\mathcal{P}, k) = \mathbf{1}_{C^i}(x_k)$. The plasma being piecewise-constant has no impact on what has to be scored here. We denote the analog estimator for the number of absorption events in an analog simulation by `a.a_abs` and for the number of scattering events by `a.a_sc`.

3.2 Collision estimator

The collision estimator does not distinguish between absorption and scattering collisions, but only samples the measure $\psi_c(x, v) dx dv$. Then,

$$\left(\frac{R_a(x)}{R_t(x)} s_{a,*}(v) + \frac{R_s(x)}{R_t(x)} \int s_{s,*}(v \rightarrow v') \hat{f}_{\text{postcol}}(v'|x) dv' \right) \mathbf{1}_{C^i}(x) \quad (3.9)$$

has to be scored for every sample to compute the integral in Eq. (3.4).

This estimator is called the collision estimator, since it boils down to counting the expected contribution due to a collision in grid cell i , at every collision regardless of its outcome. We denote collision estimators by c . Since this estimator can be combined with the analog simulation and the non-analog collision type simulations of Section 2, we obtain two collision type source term estimation procedures, which we denote by a_c , respectively na_c .

We denote the expected score of a collision at position x with pre-collision velocity v by

$$s_{c,*}(x, v) = \frac{R_a(x)}{R_t(x)} s_{a,*}(v) + \frac{R_s(x)}{R_t(x)} \int s_{s,*}(v \rightarrow v') \hat{f}_{\text{postcol}}(v'|x) dv'. \quad (3.10)$$

This factor only depends on the estimated quantity, the position where the collision takes place, and the pre-collision velocity v . Note furthermore that the integral over the post-collisional velocity v' in Eq. (3.10) is not difficult to compute: since $s_{s,*}(v \rightarrow v')$ is a simple polynomial in v' , the solution of the inner integral is a combination of moments of $\hat{f}_{\text{postcol}}^i(v')$, which are known from the plasma simulation. For instance, if the momentum is the estimated quantity, $s_{a,\text{mom}}(v) = v$ and $s_{s,\text{mom}}(v \rightarrow v') = v - v'$ and Eq. (3.10) becomes

$$s_{c,\text{mom}}(x, v) = \frac{R_a(x)}{R_t(x)} v + \frac{R_s(x)}{R_t(x)} (v - u_p(x)), \quad (3.11)$$

with $u_p(x)$ the expected post-collisional velocity at position x , a quantity that is computed by the plasma simulation.

With $s_{c,*}(x, v)$ as defined in Eq. (3.10), the scores for a collision estimator can be written as

$$s_{a,*}^{i,c}(\mathcal{P}, k) = s_{s,*}^{i,c}(\mathcal{P}, k) = s_{c,*}(x_k, v_k) \mathbf{1}_{C^i}(x_k), \quad (3.12)$$

and $s_{\text{out},*}^{i,c}(\mathcal{P}, k) = s_{r,*}^{i,c}(\mathcal{P}, k) = s_{g,*}^{i,c}(\mathcal{P}, k) = 0$.

For the non-analog collision type simulation, the only change consists in multiplying the score at each collision event k with the weight at the collision, being \bar{w}_{k-1} . The collision estimator can be used for each quantity of interest and combined with both simulation types. We illustrate this estimator with a collision estimator for momentum in an analog simulation.

Example 3.2 (Momentum estimation by an a_c estimator). We apply a collision estimator to the same case as in example 3.1, and with Eq. (3.11) and Eq. (3.12), we find

$$s_{a,\text{mom}}^{i,c}(\mathcal{P}^n, k) = s_{s,\text{mom}}^{i,c}(\mathcal{P}^n, k) = \left(\frac{R_a(x_k^n)}{R_t(x_k^n)} v_k^n + \frac{R_s(x_k^n)}{R_t(x_k^n)} (v_k^n - u_p(x_k^n)) \right) \mathbf{1}_{C^i}(x_k^n) \quad (3.13)$$

as scores at the different collisions. With Eq. (3.13) and $s_{\text{out},*}^{i,c}(\mathcal{P}^n, k) = s_{r,*}^{i,c}(\mathcal{P}^n, k) = s_{g,*}^{i,c}(\mathcal{P}^n, k) = 0$, Eq. (3.5) specifies to

$$S_{\text{mom}}^{i,c} = \sum_{n=1}^N \sum_{k=1}^{K^n} \left(\frac{R_a(x_k^n)}{R_t(x_k^n)} v_k^n + \frac{R_s(x_k^n)}{R_t(x_k^n)} (v_k^n - u_p^i) \right) c_k^n \mathbf{1}_{C^i}(x_k^n). \quad (3.14)$$

As for the analog estimator, we end the description of the collision estimator by using it to estimate the number of absorption events and the number of scattering events when the plasma is piecewise constant. First, we discuss how the collision estimator simplifies in general when the plasma is piecewise-constant. Then, we apply it to the fundamental case.

For piecewise-constant plasma the reaction rates are constants R_a^i , R_s^i , and R_t^i in each grid cell i and the post-collisional velocity distribution is a position-independent function $\hat{f}_{\text{postcol}}^i(v')$. We use these constants and this position-independent function to simplify the factor $s_{c,*}(x, v)$ in the scores by the collision estimator, Eq. (3.12), as

$$s_{c,*}(x, v) \mathbf{1}_{C^i}(x) = s_{c,*}^i(v) \mathbf{1}_{C^i}(x) = \left(\frac{R_a^i}{R_t^i} s_{a,*}(v) + \frac{R_s^i}{R_t^i} \int s_{s,*}(v \rightarrow v') \hat{f}_{\text{postcol}}^i(v') dv' \right) \mathbf{1}_{C^i}(x). \quad (3.15)$$

Fundamental cases. Applying the collision estimator for the number of absorption events and the number of scattering events when the plasma background is piecewise-constant, amounts to scoring a constant at every collision. Hence, when applying these two estimators to the same simulation, the result only differs by a constant. Consequently, the statistical properties of a collision estimator for the expected number of absorption events and for the expected number of scattering events are identical, and shared by a collision estimator for the expected total number of collisions. We thus restrict ourselves to only considering one of these fundamental cases, namely a collision estimator for the total number of collisions, which amounts to scoring the particle weight at every collision.

4 Derivation of the ODEs for the estimation procedure performance using invariant imbedding

In the previous two sections, we arrived at several source term estimation procedures: the basic estimation procedures a_a.abs and a_a.scnt, and the competing estimation procedures for the expected total number of collisions, a_c, and nac_c. The goal of this paper

is to provide a quantitative analysis of these estimators based on the parameters of the problem. In this Section we discuss the method used to compare the estimation procedures, the results of which are shown in Section 5.

To do so, we simplify the model problem in Section 4.1 to a situation with only forward-backward scattering and constant rates. We denote this simplified model as the 1D0D problem, since it is one-dimensional in space, but zero-dimensional in velocity. The performance of the estimation procedures is measured in both relative statistical error (given a number of simulated particles) and the computational cost (given a certain statistical error). For each of the estimation procedures, it is possible to construct sets of ODEs that allow computation of both measures of performance in the 1D0D problem. The method used for this is called invariant imbedding. It is discussed in Section 4.2.1 and illustrated in Section 4.2.2. For the full derivation of all the ODEs (which is extremely lengthy), we refer to the Technical Report [19].

4.1 1D0D simplification

To facilitate an analytical study of the performance of the different estimation procedures, we simplify the one-dimensional model to only have forward-backward scattering. Concretely, we restrict the velocity to being ± 1 , making the model zero-dimensional in velocity. The post-collisional velocity distribution is then completely determined by one parametric value: the probability of going right after a collision, p_r . This reduces the post-collision velocity distribution to

$$\hat{f}_{\text{postcol}}^{1\text{D}0\text{D}}(v) = p_r \delta(v-1) + (1-p_r) \delta(v+1), \quad (4.1)$$

with δ the Dirac-delta. The constant size of the velocity and the space-independence of the rates, result in constant cross-sections Σ_a and Σ_s which can be used instead of the reaction rates (see Remark 2.3). With all the particles entering from the left, the initial velocity distribution is also reduced to

$$\hat{f}_0^{1\text{D}0\text{D}}(v) = \delta(v-1). \quad (4.2)$$

Furthermore, we take the probability of being reflected equal to be 0 at each end of the domain, hence $\alpha(r) \equiv 1$.

This reduces the investigated parameter space to three dimensions: the survival probability at a collision Σ_a/Σ_t , the dedimensionalized total collision rate $\Sigma_t L$ and the post-collisional parameter p_r .

The constant size of the velocity in this simplification has as an additional effect that energy of the particles always remains proportional to their mass. This means the energy source estimates are proportional to the mass source estimate and consequently that their performance is identical, meaning that the results for mass source estimation that we attain by this method hold for energy source estimation as well.

4.2 Invariant imbedding procedure

4.2.1 Principle

For the simplified 1D0D model of Section 4.1, we can derive ODEs to calculate both the variance and the expected computational cost for a given statistical error, which feature as measures of performance. The invariant imbedding procedure [1,2] consists of writing the moment of a quantity, the score for example, for a slab of length x that is extended to a slab of length $x + \Delta x$ as a function of moments of quantities for a slab of length x and its extension Δx . By taking the limit of $\Delta x \rightarrow 0$, an ODE is formed with the domain length as an integration variable. For the other quantities that arise, a similar procedure can be followed, until the set of ODEs is closed.

For each of the estimation procedures, this invariant imbedding procedure leads to a system of ODEs. In each of these ODE systems the parameters $(\Sigma_a, \Sigma_s, p_r)$ are fixed, and the domain length x is the integration variable.

4.2.2 Invariant imbedding example

To illustrate the procedure, we include part of the invariant imbedding procedure of the non-analog collision type collision estimation procedure (nac_c). More details, as well as the derivations for all other estimator-simulation combinations are described in detail in the Technical Report [19].

A non-analog collision type simulation (nac) executes every collision as a scattering event, keeping the simulation unbiased by reweighing the particle by a factor Σ_s/Σ_t at every collision, see Section 2.3. The final weight change of a particle in an nac simulation after it passed through a domain of length x , in which multiple collisions might have taken place, is denoted by $\bar{W}(x)$. As discussed in Section 3.2, a collision estimator for the expected number of collisions, scores 1 at every collision. To estimate the expected number of a certain type of collisions, instead of 1, Σ_a/Σ_t is scored for absorption events, respectively by Σ_s/Σ_t for scattering events. To clarify the use of cross-sections in our derivation, we denote the score at every collision as Σ/Σ_t . The total score by an nac_c estimation procedure by a single particle path through a domain of length x is denoted by $\bar{C}(x)$.

Here, we will focus on the second moment of the score of an nac_c estimation procedure, an indispensable quantity to compute its variance. We consider here the contribution by paths that leave and enter the domain from the left. Other outcomes are treated similarly. We denote the outcome by a subscript of two letters, of which the first denotes the place of entry and the second the place of exit. The probability of a path under the condition that it enters and leaves from the left is denoted by $\bar{P}_{ll}(x)$.

The quantity we focus on here is $\bar{P}_{ll}(x)\mathbb{E}[\bar{C}^2(x)]$, the contribution to the second moment of a collision estimator in a non-analog collision type simulation in a domain of length x by the particle paths that enter and leave from the left. To do so, we will express $\bar{P}_{ll}(x + \Delta x)\mathbb{E}[\bar{C}^2(x + \Delta x)]$, as a function of quantities over x . To this end, we condition the paths that enter and leave the domain of length $x + \Delta x$ from the left by their behaviour

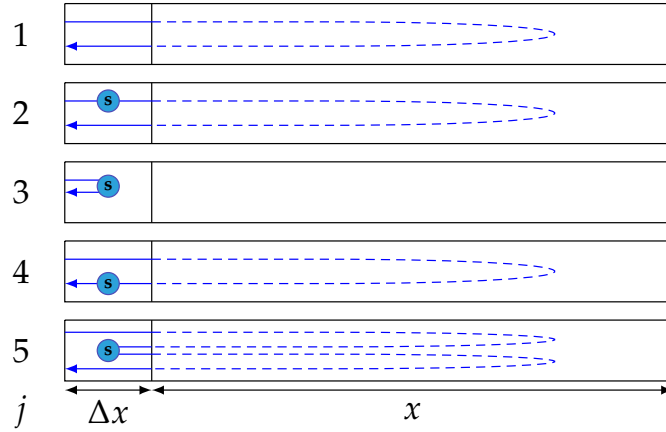


Figure 2: The possible paths in a domain of length $x + \Delta x$ that start and end on the left side in a non-analogous simulation and have a probability of order at most 1 in Δx . The symbol \bullet in the part of length Δx identifies that a collision took place there. The dashed lines in the x part of the domain signify that the behaviour there is irrelevant, as long as the outcome is correct: entering and leaving the x part from the left.

in the part of Δx . Since our aim is to arrive at an ODE for $\bar{P}_{ll}(x)\mathbb{E}[\bar{C}^2(x)]$, we can neglect contributions to $\bar{P}_{ll}(x + \Delta x)\mathbb{E}[\bar{C}^2(x + \Delta x)]$ of order $o(\Delta x)$, $\Delta x \rightarrow 0$. Hence, we can neglect paths that collide more than once in the Δx part of the domain, since these would occur with a probability of order $\mathcal{O}(\Delta x^2)$, $\Delta x \rightarrow 0$, because when travelling a length of $\Delta x \rightarrow 0$ the probability of colliding is $\Sigma_t \Delta x$, $\Delta x \rightarrow 0$. When restricting the outcome of the paths to leaving and entering from the left, and to having at most one collision in the Δx part of the domain, there are five options left of how the particle can act within the domain of length Δx , which are shown in Fig. 2.

With j referring to the cases in Fig. 2, we can write

$$\bar{P}_{ll}(x + \Delta x)\mathbb{E}[\bar{C}_{ll}(x + \Delta x)] = \sum_{j=1}^5 \bar{P}_{ll,j}(x + \Delta x)\mathbb{E}[\bar{C}_{ll,j}^2(x + \Delta x)], \quad (4.3)$$

by Taylor expansion of the exponential. We now explicitly work out $\bar{P}_{ll,4}$ and $\mathbb{E}[\bar{C}_{ll,4}]$, after which we will provide all five terms and show how this leads to an ODE.

In the first case of Fig. 2, the particle does not collide in the Δx part of the domain after its entry, returns to the Δx part as the outcome of its passage through the x part of the domain and, then collides in the Δx part, after which it exits the domain of length $x + \Delta x$. The probability of this case is thus

$$\bar{P}_{ll,4}(x + \Delta x) = \left(1 - e^{-\Sigma_t \Delta x}\right) \bar{P}_{ll}(x) e^{-\Sigma_t \Delta x} p_l, \quad (4.4)$$

the probability of not colliding when passing through the Δx part for the first time, times the probability of returning to the Δx part, times the probability of colliding in the second

passage through the Δx part and going left after the collision. Since we can neglect all contributions of $o(\Delta x)$, $\Delta x \rightarrow 0$, we write

$$\bar{P}_{ll,A}(x + \Delta x) = \bar{P}_{ll}(x) \Sigma_t \Delta x p_l + \mathcal{O}(\Delta x^2), \quad \Delta x \rightarrow 0. \quad (4.5)$$

The score by a particle conditioned on the first case equals

$$\bar{C}_{ll,1}(x + \Delta x) = \bar{C}_{ll}(x) + \bar{W}_{ll}(x) \frac{\Sigma}{\Sigma_t}, \quad (4.6)$$

and thus the second moment conditioned on that case is equal to

$$\mathbb{E} \left[\left(\bar{C}_{ll}(x) + \bar{W}_{ll}(x) \frac{\Sigma}{\Sigma_t} \right)^2 \right] = \mathbb{E} [\bar{C}_{ll}^2(x)] + 2 \frac{\Sigma}{\Sigma_t} \mathbb{E} [\bar{C}_{ll}(x) \bar{W}_{ll}(x)] + \frac{\Sigma^2}{\Sigma_t^2} \mathbb{E} [\bar{W}_{ll}^2(x)]. \quad (4.7)$$

The new quantities on the right hand side of Eq. (4.7), $\mathbb{E}[\bar{C}_{ll}(x) \bar{W}_{ll}(x)]$ and $\mathbb{E}[\bar{W}_{ll}^2(x)]$ are all at most second-order in the path variables ($\bar{C}_{ll}(x)$ and $\bar{W}_{ll}(x)$), as is the quantity, $\mathbb{E}[\bar{C}_{ll}^2(x + \Delta x)]$, we are after. This feature of the invariant imbedding procedure is true for all our derivations, and allows to find a closed set of ODEs, since the number of second-order moments we can take is finite and each of them depends on moments of at most second order.

With Eqs. (4.5) and (4.7) we can find the fourth term of the right hand side of Eq. (4.3) as

$$\begin{aligned} \text{term 4} = & \bar{P}_{ll}(x) \Sigma_t \Delta x p_l \left(\mathbb{E} [\bar{C}_{ll}^2(x)] + 2 \frac{\Sigma}{\Sigma_t} \mathbb{E} [\bar{C}_{ll}(x) \bar{W}_{ll}(x)] + \frac{\Sigma^2}{\Sigma_t^2} \mathbb{E} [\bar{W}_{ll}^2(x)] \right) \\ & + \mathcal{O}(\Delta x^2), \quad \Delta x \rightarrow 0, \end{aligned} \quad (4.8)$$

For the other four terms of Eq. (4.3), one can work similarly (see the Technical Report [19]), taking into account that at collisions the particle is reweighed by a factor Σ_s / Σ_t . The results for the remaining four cases are

$$\text{term 1} = \bar{P}_{ll}(x) (1 - 2 \Sigma_t \Delta x) \mathbb{E} [\bar{C}_{ll}^2(x)] + \mathcal{O}(\Delta x^2), \quad \Delta x \rightarrow 0, \quad (4.9)$$

$$\text{term 2} = \Sigma_t \Delta x p_r \bar{P}_{ll}(x) \left(\frac{\Sigma^2}{\Sigma_t^2} + 2 \frac{\Sigma_s \Sigma}{\Sigma_t^2} \mathbb{E} [\bar{C}_{ll}(x)] + \frac{\Sigma_s^2}{\Sigma_t^2} \mathbb{E} [\bar{C}_{ll}^2(x)] \right) + \mathcal{O}(\Delta x^2), \quad \Delta x \rightarrow 0, \quad (4.10)$$

$$\text{term 3} = p_l \frac{\Sigma^2}{\Sigma_t} \Delta x + \mathcal{O}(\Delta x^2), \quad \Delta x \rightarrow 0, \quad (4.11)$$

$$\begin{aligned} \text{term 5} = & \bar{P}_{ll}(x) \Sigma_t \Delta x p_r \bar{P}_{ll}(x) \left(\mathbb{E} [\bar{C}_{ll}^2(x)] + 2 \frac{\Sigma}{\Sigma_t} \mathbb{E} [\bar{W}_{ll}(x) \bar{C}_{ll}(x)] \right. \\ & + 2 \frac{\Sigma_s}{\Sigma_t} \mathbb{E} [\bar{W}_{ll}(x) \bar{C}_{ll}(x)] \mathbb{E} [\bar{C}_{ll}] + \frac{\Sigma}{\Sigma_t} \mathbb{E} [\bar{W}_{ll}^2(x)] + \frac{\Sigma_s^2}{\Sigma_t^2} \mathbb{E} [\bar{W}_{ll}^2(x)] \mathbb{E} [\bar{C}_{ll}^2(x)] \\ & \left. + 2 \frac{\Sigma \Sigma_s}{\Sigma_t^2} \mathbb{E} [\bar{W}_{ll}^2(x) \bar{C}_{ll}(x)] \right) + \mathcal{O}(\Delta x^2), \quad \Delta x \rightarrow 0. \end{aligned} \quad (4.12)$$

Substituting the five terms in Eq. (4.3) gives an expression for $\bar{P}_{ll}(x + \Delta x)\mathbb{E}[\bar{C}_{ll}^2(x + \Delta x)]$, which, by dividing by Δx and taking the limit $\Delta x \rightarrow 0$, can be transformed into an ordinary differential equation for the quantity $\bar{P}_{ll}\mathbb{E}[\bar{C}_{ll}^2]$,

$$\begin{aligned} & \frac{d(\bar{P}_{ll}(x)\mathbb{E}[\bar{C}_{ll}^2(x)])}{dx} \\ &= -2\Sigma_t\bar{P}_{ll}(x)\mathbb{E}[\bar{C}_{ll}^2(x)] + p_r\frac{\Sigma_t^2}{\Sigma_t}\bar{P}_{ll}(x) + 2p_r\frac{\Sigma\Sigma_s}{\Sigma_t}\bar{P}_{ll}(x)\mathbb{E}[\bar{C}_{ll}(x)] \\ & \quad + p_r\frac{\Sigma_s^2}{\Sigma_t}\bar{P}_{ll}(x)\mathbb{E}[\bar{C}_{ll}^2(x)] + p_l\frac{\Sigma^2}{\Sigma_t} + p_l\Sigma_t\bar{P}_{ll}(x)\mathbb{E}[\bar{C}_{ll}^2(x)] + 2p_l\Sigma\bar{P}_{ll}(x)\mathbb{E}[\bar{W}_{ll}(x)\bar{C}_{ll}(x)] \\ & \quad + p_l\frac{\Sigma^2}{\Sigma_t}\bar{P}_{ll}(x)\mathbb{E}[\bar{W}_{ll}^2(x)] + p_r\Sigma_t\bar{P}_{ll}(x)\bar{P}_{ll}(x)\mathbb{E}[\bar{C}_{ll}^2(x)] + 2p_r\Sigma\bar{P}_{ll}(x)\bar{P}_{ll}(x)\mathbb{E}[\bar{W}_{ll}(x)\bar{C}_{ll}(x)] \\ & \quad + 2p_r\Sigma_s\bar{P}_{ll}(x)\mathbb{E}[\bar{W}_{ll}(x)\bar{C}_{ll}(x)]\bar{P}_{ll}(x)\mathbb{E}[\bar{C}_{ll}(x)] + p_r\Sigma\bar{P}_{ll}(x)\bar{P}_{ll}(x)\mathbb{E}[\bar{W}_{ll}^2(x)] \\ & \quad + p_r\frac{\Sigma_s^2}{\Sigma_t}\bar{P}_{ll}(x)\mathbb{E}[\bar{W}_{ll}^2(x)]\bar{P}_{ll}(x)\mathbb{E}[\bar{C}_{ll}^2(x)] + 2p_r\frac{\Sigma\Sigma_s}{\Sigma_t}\bar{P}_{ll}(x)\mathbb{E}[\bar{W}_{ll}^2(x)]\bar{P}_{ll}(x)\mathbb{E}[\bar{C}_{ll}(x)], \quad (4.13) \end{aligned}$$

which equals Equation (60) in the Technical Report [19]. The initial value to solve this ODE is 0, because the probability of turning in a slab of length zero is zero, hence so is $\bar{P}_{ll}(0)$ and $\mathbb{E}[\bar{C}_{ll}^2(0)]$.

The same procedure can be applied recursively for each of the terms appearing here, eventually leading to a closed set of ODEs. The full details of this derivation (and all other derivations for the other estimation procedures) are included in the Technical Report [19].

To evaluate the estimation procedures for a set of the non-dimensional parameters as introduced in Section 4.1 (Σ_s/Σ_t , $\Sigma_t L$, p_r), the ODEs are to be evaluated until $x = L$. In doing so, we also find the results for smaller values of L . Hence, to find the measure of performance of the estimation procedures on a fine mesh of parameter values, we have to integrate these ODEs as our mesh has values of Σ_s/Σ_t and p_r and integrate them with a step length and final value, determined by the desired values of $\Sigma_t L$.

5 Comparison of the estimation procedures in 1D0D

For each of the estimation procedures, we have evaluated the statistical error and the computational cost throughout the parameter space of the 1D0D problem by numerically evaluating the ODEs constructed with the invariant imbedding procedure as discussed in Section 4 and included in the Technical Report [19].

An alternative to compute the performance of the different estimation procedures in the parameter space, is using multiple MC experiments for each parameter set and computing both measures of performance. This method is of limited use because estimating the relative statistical error and the computational cost sufficiently accurately is computationally expensive for every parameter set. Even in the three-dimensional parameter space introduced in Section 4.1, computing these quantities for a fine mesh of parameter

values is infeasible. We do use individual MC simulations to compute the performance of the different estimation procedures, but only on a coarse mesh of parameter values. Individual MC simulations have been used in our work to validate the analytical results of the invariant imbedding method.

In Sections 5.1 and 5.2, we solve the ODE systems originating from the invariant imbedding procedure to discuss the impact of the problem parameters (the total collisionality $\Sigma_t L$, the survival probability Σ_a/Σ_t and the anisotropy p_r) on the performance of the different estimation procedures. These effects can be easily understood, but the exact trade-off is non-trivial. In paper, we restrict ourselves to a discussion of the performance of analog and collision estimation procedure individually as a function of the scattering rate and ionization rate. In future work, we will consider additional, more advanced estimation procedures, and perform a detailed comparison on a realistic test case.


5.1 Relative standard deviation

We first compare the different estimation procedures based on the relative standard deviation. If the number of particles entering the domain is given, the relative standard deviation is a measure for the relative statistical error.

In Section 5.1.1 we first focus on the case with trivial scattering: $p_r = 1$, for particles entering from the left. Doing so allows to explain most of the effects that determine the performance of the different estimation procedures. In Section 5.1.2 we discuss how these effects are deformed in the case of non-trivial scattering.

5.1.1 Trivial scattering, $p_r = 1$

If $p_r = 1$, the scattering is trivial: the particles never change velocity since the post-scattering velocity is always 1, which is also the velocity at which the particles enter the simulation. In this setting, the mechanisms at hand are still very clear. Still, even in this simple situation, it is nontrivial which of the mechanisms dominates for which parameter set, and what the quantitative results are. To attain that, ODEs as derived with invariant imbedding are necessary and this simple situation with trivial scattering often has easily obtainable analytic solutions for the ODEs, as has been done by [17] for, among others, `a_a_abs` and `a_c`. In this section, we incorporate these results and complement them with the additional estimation procedures, `a_a_sc` and `na_c`. The results in this section form a stepping stone towards the rest of our results which, to the best of our knowledge, are completely new.

Fig. 3 shows the results of this part and includes a graph for each of the four estimation procedures. Below, we refer to the position of the estimation procedure with a pictogram , where the correct position is coloured. The axes of these figures are the non-dimensional scattering and absorption cross-sections of which combinations are taken up to $\Sigma_t L = 10$. For larger values of $\Sigma_t L$, the contour lines become invariant to L ,

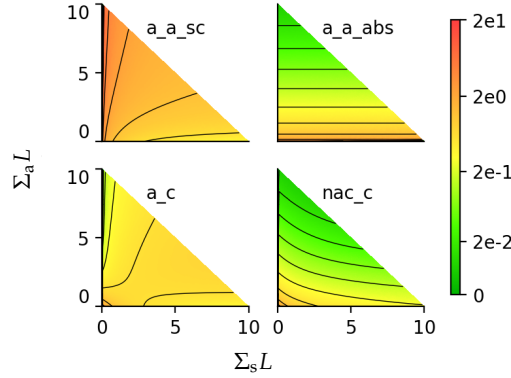
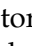
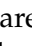
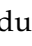


Figure 3: Relative standard deviation for different simulation-estimator combinations with $p_r = 1$.

so they become straight lines. This is because, with large collision probabilities, the probability of a particle reaching the end of the domain is very small, so their contribution becomes negligible. Since particles reaching the end constitute a negligible part, making the domain larger has no effect. In the discussion below, the different estimation procedures are indicated by pictograms that refer to the ordering of the combinations in the figure.

The analog absorption estimator (a_a_abs , ) is one of the most trivial estimators, both in how it works and in the resulting figure. The statistical error is independent of the scattering rate since the scattering events do not contribute to the estimate and, if $p_r = 1$, the scattering collisions furthermore do not impact the particle weight, nor the trajectory. If $\Sigma_a L$ increases, the statistical error decreases, since it steadily becomes almost certain that the particle will be absorbed.

The analog scattering estimator (a_a_sc , ) behaves completely differently compared to the absorption estimator. Now the scattering events constitute scoring events, without having any other impact, meaning that an increase of the scattering rate $\Sigma_s L$ improves the variance. The occurrence of absorption events now has an adverse effect, since it introduces a variable length and thus an increased variance in the amount of scattering events that take place.

A much more complex situation is visible in the analog collision estimation procedure (a_c , ) which combines traits of the analog scattering estimator and the analog absorption estimator. It scores the same at both scattering and absorption events, so increasing either $\Sigma_s L$ or $\Sigma_a L$, increases the amount of scored events. In some instances it decreases the variance but in others it increases. First, when scattering is dominant, increasing $\Sigma_a L$ increases the variance. This is a result of the increased variability of the path length and thus of the amount of scattering events at which scoring takes place, an argument we encountered when discussing the a_a_sc estimation procedure. Secondly, when absorption is dominant, the variance increases when the amount of scattering increases. This can be understood from the extreme situation with very high absorption and no scattering.

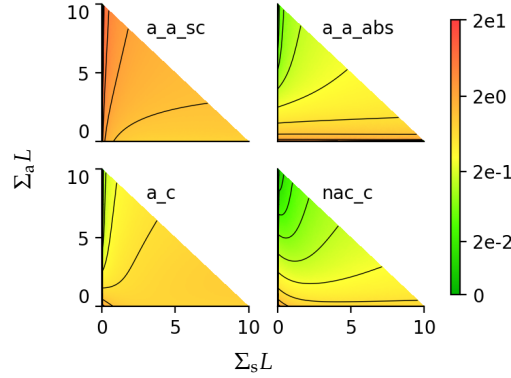


Figure 4: The relative standard deviation for the different simulation-estimator combinations with $p_r=0.75$.

Then, the variance is nearly zero due to the single, ‘almost certain’ absorption. Adding scattering to this situation, introduces variance on the amount of events that occur.

In the non-analog collision type collision estimator (nac_c , \blacksquare), all events have an identical effect, both on the particle path and on the scoring. The only thing that is now stochastic, is the amount of these equivalent collisions. Increasing the amount of collisions consequently improves the variance. The picture is not symmetric however, due to the fact that the weight is multiplied by the survival probability after every collision. If the survival probability is lower, the later collisions are less significant, and since there is more variability in the occurrence of these, an increase of $\Sigma_a L$ is more positive for the variance than an increase of $\Sigma_s L$.

5.1.2 Non-trivial scattering

The setting with trivial scattering served to introduce most of the effects at play. Now, when the particle can change direction upon scattering, these effects drastically deform and are supplemented with several new effects. We will introduce these in Fig. 4 where the probability of going right after a scattering event, p_r , equals 0.75.

Again, the analog absorption estimator (\blacksquare) provides a good starting point. In contrast to the situation with trivial scattering (Fig. 3, \blacksquare), scattering collisions do influence the path of the particle now. This is a new source of stochasticity and increases the variance of the score. This new negative effect of non-trivial scattering is visible in every subfigure, as can be seen by comparing Fig. 4 with Fig. 3 and is to be compared with the other effects an increase in the scattering has and were discussed in the previous section.

Especially for the two collision estimation procedures we consider here (\blacksquare), this complicates the picture significantly. Now the effect of an increase in $\Sigma_s L$ on the statistical error is no longer monotonous. For both, there are values of $\Sigma_a L$ to be found for which there is first a decrease of the variance and then an increase. The reason lies in the ever-increasing complexity of the path, which after a certain time dominates the initial decrease in variance due to extra scoring moments.

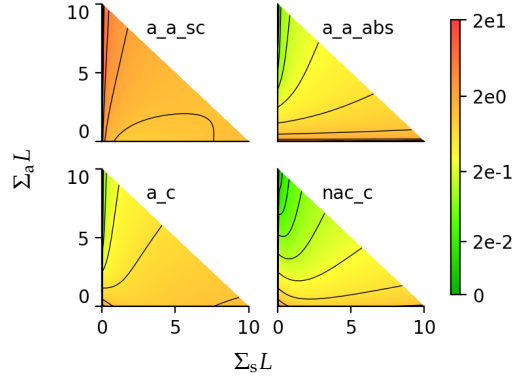


Figure 5: The relative standard deviation for the different simulation-estimator combinations with $p_r = 0.5$.

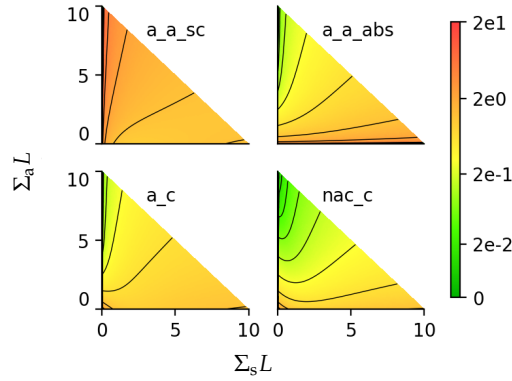


Figure 6: The relative standard deviation for the different simulation-estimator combinations with $p_r = 0.25$.

Other values of p_r than 1 or 0.75 do not show other effects, but the specific trade-off between the different effects at play changes. Different values are shown in Figs. 5, 6 and 7.

5.2 Computational cost

Using the invariant imbedding procedure, we can also find and solve ODEs for the expected computational cost for a given statistical error. The statistical error equals σ / \sqrt{N} with σ the standard deviation of a single particle and N the number of simulated particles. We assume that the simulation cost per particle is dominated by the execution of collisions, resulting in a simulation cost for a given statistical error that scales as

$$\sigma^2 \mathbb{E}[\text{collisions per path}]. \quad (5.1)$$

The expected number of collisions per path is independent of the chosen estimator, but solely depends on the simulation type (a or nac). For the analog simulation (a), only the

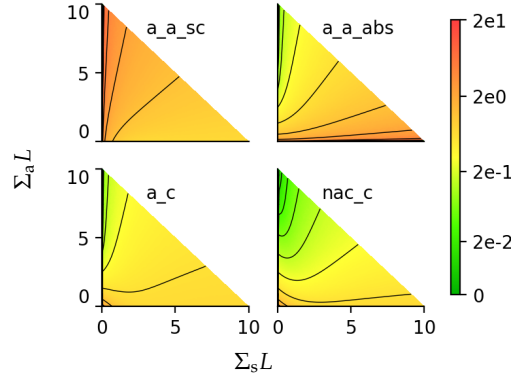


Figure 7: The relative standard deviation for the different simulation-estimator combinations with $p_r = 0$.

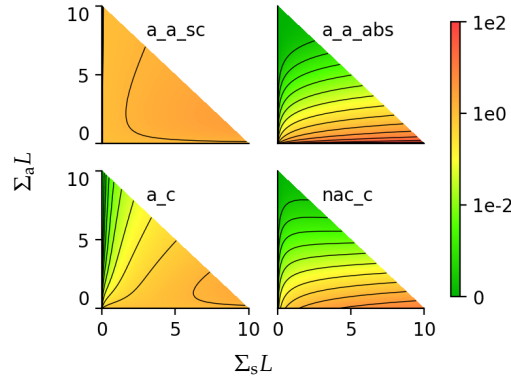


Figure 8: A measure of computational cost for the different simulation-estimator combinations with $p_r = 1$.

physical scattering collisions, determined by the cross-section Σ_s have to be simulated as such. The absorption collision cuts the path and keeps the computational cost down. In the non-analog collision type simulation (nac) all collisions are simulated as if they are scattering collisions, meaning the cost increases in comparison to the analog simulation case.

We show the resultant computational cost measure for each of the simulation types and for values of $p_r \in \{1, 0.5, 0\}$ in Figs. 8 to 10.

For the estimation procedures with an analog simulation (\blacksquare), this means increased scattering has as the additional effect of increasing the simulation cost. This shows itself most clearly by comparing Fig. 3 to Fig. 8. For each estimation procedure, increasing the scattering rate has an additional adverse effect.

For the non-analog collision type simulation (\blacksquare) this additional adverse effect is also present when the absorption rate increases, although this is clouded by the previously discussed drop in variance.

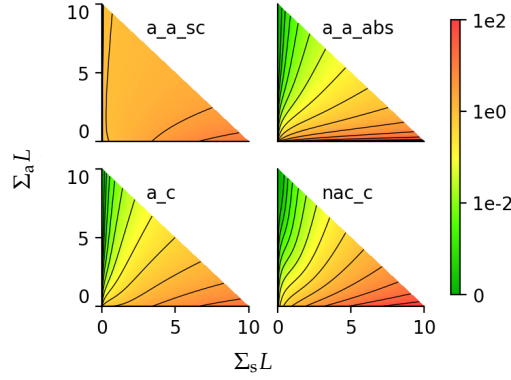


Figure 9: A measure of computational cost for the different simulation-estimator combinations with $p_r=0.5$.

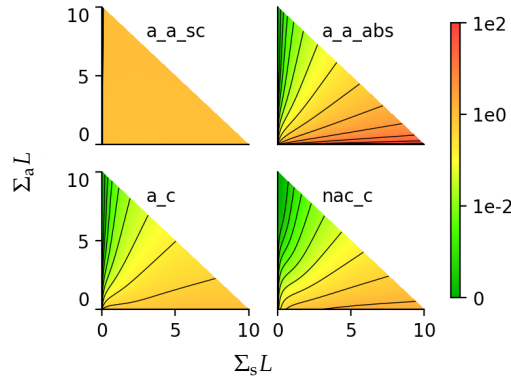


Figure 10: A measure of computational cost for the different simulation-estimator combinations with $p_r=0$.

Note that the ever increasing cost for the non-analog simulations with increasing $\Sigma_t L$ can in practice be avoided by using techniques like Russian roulette or weight cut-off [25].

6 Conclusion and future prospects

In this paper, we provide an extensive analysis of source term estimation procedures in coupled finite-volume/Monte-Carlo methods. We first established the framework which we use to derive the estimation procedures and prove their unbiasedness. We used this framework to establish the more basic estimation procedures: the analog and collision estimators for the analog simulation and the extension of the collision estimator to a different simulation type, where absorption events are executed via weight loss at collisions. For these estimation procedures, we performed an analytical study for the mass source estimation in a simplified 1D0D setting with a forward-backward scattering model and the occurrence of only a single velocity. The simplifications of the 1D0D setting allow

for an analytical study of the performance by using an invariant imbedding methodology, which we explained and illustrated with an example. The full derivations are in the Technical Report [19].

This analytical study provides the performance in terms of both statistical error and computational cost for each estimation procedure throughout the parameter domain, thereby extending existing analyses of the estimation procedures substantially. These results allow to clearly uncover the mechanisms that determine the parameter dependence of the estimation procedures and how these mechanisms balance out in a quantitative manner.

In future work, we will extend our methodology to other, more advanced estimation procedures, and we will provide a full comparison and several numerical extensions to establish which estimation procedure is competitive under different conditions.

Acknowledgments

This work has been carried out within the framework of the EUROfusion Consortium and has received funding from the Euratom research and training programme under grant agreements No. 633053 and No. 101052200. Views and opinions expressed are however those of the author(s) only and do not necessarily reflect those of the European Union or the European Commission. Neither the European Union nor the European Commission can be held responsible for them. Parts of the work are supported by the Research Foundation Flanders (FWO) under project grant G078316N. The first author is funded by a PhD fellowship of the Research Foundation Flanders (FWO). The computational resources and services used in this work were provided by the VSC (Flemish Supercomputer Center), funded by the Research Foundation - Flanders (FWO) and the Flemish Government – department EWI.

References

- [1] Richard Bellman and George Milton Wing. *An Introduction to Invariant Imbedding*. John Wiley & Sons Inc, 1975.
- [2] Subrahmanyan Chandrasekhar. *Radiative Transfer*. Oxford University Press, 1950.
- [3] John M Dawson. Particle simulation of plasmas. *Reviews of Modern Physics*, 55(2):403, 1983.
- [4] Y Feng, F Sardei, P Grigull, K McCormick, J Kisslinger, D Reiter, and Y Igitchkanov. Transport in island divertors: Physics, 3D modelling and comparison to first experiments on W7-AS. *Plasma Physics and Controlled Fusion*, 44(5):611, 2002.
- [5] ME Fenstermacher, GD Porter, ME Rensink, TD Rognlien, SL Allen, DN Hill, CJ Lasnier, T Leonard, and T Petrie. UEDGE and DEGAS modeling of the DIII-D scrape-off layer plasma. *Journal of Nuclear Materials*, 220:330–335, 1995.
- [6] Kristel Ghooos, Wouter Dekeyser, Giovanni Samaey, Petra Börner, Detlev Reiter, and Martine Baelmans. Accuracy and convergence of coupled finite-volume/Monte-Carlo codes for plasma edge simulations. *Contributions to Plasma Physics*, 56(6-8):616–621, 2016.

- [7] R Indira. Analytical study of leakage estimators in Monte-Carlo simulation of radiation transport. *Annals of Nuclear Energy*, 15(5):261–269, 1988.
- [8] R Indira. Optimization of biasing parameters in particle transport simulations. *Annals of Nuclear Energy*, 16(11):571–576, 1989.
- [9] R Indira and TM John. Variance reduction under exponential and scattering angle biasing: An analytic approach. *Nuclear Science and Engineering*, 94(4):323–336, 1986.
- [10] James Juno, Ammar Hakim, Jason TenBarge, E Shi, and William Dorland. Discontinuous Galerkin algorithms for fully kinetic plasmas. *Journal of Computational Physics*, 353:110–147, 2018.
- [11] Herman Kahn. Applications of Monte Carlo. 1956.
- [12] AS Kukushkin, HD Pacher, V Kotov, GW Pacher, and D Reiter. Finalizing the ITER divertor design: The key role of SOLPS modeling. *Fusion Engineering and Design*, 86(12):2865–2873, 2011.
- [13] I Lux. Remark on the theory of nonanalog Monte-Carlo games. *Atomkernenergie*, 31(3):154–155, 1978.
- [14] I Lux. Systematic study of some standard variance reduction techniques. *Nuclear Science and Engineering*, 67(3):317–325, 1978.
- [15] Iván Lux. Variance and efficiency in transport, Monte Carlo report KFKI-1979-35. Technical report, Central Research Institute for Physics, Budapest, Hungary, 1979.
- [16] Ivan Lux and László Koblinger. *Monte Carlo Particle Transport Methods: Neutron and Photon Calculations*, volume 102. Citeseer, 1991.
- [17] DB MacMillan. Comparison of statistical estimators for neutron Monte Carlo calculations. *Nuclear Science and Engineering*, 26(3):366–372, 1966.
- [18] Luc Mieussens. Discrete-velocity models and numerical schemes for the Boltzmann-BGK equation in plane and axisymmetric geometries. *Journal of Computational Physics*, 162(2):429–466, 2000.
- [19] Bert Mortier, Martine Baelmans, and Giovanni Samaey. Invariant imbedding applied to source term estimation procedures in a simplified 1D0D slab case. Technical report, KU Leuven, 2020. <https://lirias.kuleuven.be/handle/123456789/658345>.
- [20] D Reiter, Martine Baelmans, and P Börner. The EIRENE and B2-EIRENE codes. *Fusion Science and Technology*, 47(2):172–186, 2005.
- [21] Mathias Rousset and Giovanni Samaey. Simulating individual-based models of bacterial chemotaxis with asymptotic variance reduction. *Mathematical Models and Methods in Applied Sciences*, 23(12):2155–2191, 2013.
- [22] PK Sarkar and MA Prasad. Prediction of statistical error and optimization of biased Monte Carlo transport calculations. *Nuclear Science and Engineering*, 70(3):243–261, 1979.
- [23] Clell J Solomon, Avneet Sood, Thomas E Booth, and J Kenneth Shultis. Verification of the history-score moment equations for weight-window variance reduction. In *Proceedings of the International Conference on Mathematics and Computational Methods Applied to Nuclear Science and Engineering (M&C 2011)*, Rio de Janeiro, RJ, Brazil, 2011.
- [24] Jerome Spanier. An analytic approach to variance reduction. *SIAM Journal on Applied Mathematics*, 18(1):172–190, 1970.
- [25] Jerome Spanier and Ely M Gelbard. *Monte Carlo Principles and Neutron Transport Problems*. Addison-Wesley Publishing Company, 1969.
- [26] Peter C Stangeby. *The Plasma Boundary of Magnetic Fusion Devices*, volume 224. Institute of Physics Publishing Bristol, 2000.
- [27] Daren Stotler and Charles Karney. Neutral gas transport modeling with DEGAS 2. *Contri-*

- Contributions to Plasma Physics*, 34(2-3):392–397, 1994.
- [28] Quanhua Sun, Iain D Boyd, and Graham V Candler. A hybrid continuum/particle approach for modeling subsonic, rarefied gas flows. *Journal of Computational Physics*, 194(1):256–277, 2004.
- [29] B Viola, G Corrigan, D Harting, G Maddaluno, M Mattia, V Pericoli Ridolfini, and R Zagórski. Preliminary comparison of the conventional and quasi-snowflake divertor configurations with the 2D code EDGE2D/EIRENE in the FAST tokamak. *Contributions to Plasma Physics*, 54(4-6):459–463, 2014.
- [30] Sven Wiesen, Detlev Reiter, Vladislav Kotov, Martine Baelmans, Wouter Dekeyser, AS Kukushkin, SW Lisgo, RA Pitts, Vladimir Rozhansky, Gabriella Saibene, et al. The new SOLPS-ITER code package. *Journal of Nuclear Materials*, 463:480–484, 2015.